ST SEVIER

Contents lists available at SciVerse ScienceDirect

Optics Communications

journal homepage: www.elsevier.com/locate/optcom



Investigation on the escaped and trapped emission in organic light-emitting devices

Shixiong Liang ^{a,b}, Zhaoxin Wu ^{a,b,*}, Xuanke Zhao ^{a,b}, Dawei Wang ^{a,b}, Xun Hou ^{a,b}, Zhijian Chen ^c, Oihuang Gong ^c

- a Key Laboratory of Photonics Technology for Information, School of Electronic and Information Engineering, Xi'an Jiaotong University, Xi'an, 710049, PR China
- b Key Laboratory for Physical Electronics and Devices of the Ministry of Education, School of Electronic and Information Engineering, Xi'an Jiaotong University, Xi'an, 710049, PR China
- ^c State Key Laboratory for Mesoscopic Physics and Department of Physics, Peking University, Beijing, 100871, PR China

ARTICLE INFO

Article history:
Received 31 August 2011
Received in revised form 18 November 2011
Accepted 21 November 2011
Available online 4 December 2011

Keywords:
Organic light-emitting devices
External coupling efficiency
Integrating sphere
Electric dipole

ABSTRACT

The escaped and trapped emission of small molecule based bottom emission organic light-emitting diodes was investigated by using an integrating sphere and a fiber spectrometer and a glass hemisphere. It was found that the maximum external coupling ratio $r_{\rm ext}$, namely the ratio of escaped emission to the emission of escaped and trapped in the substrate, is 56%. We also extended the "half-space" dipole model by taking dipole radiation pattern into account, which agreed well with our experiments. Our experimental and theoretical results will benefit the optimization of device structures for the higher out-coupling efficiency.

© 2011 Elsevier B.V. All rights reserved.

1. Introduction

Organic light emitting devices (OLEDs) are receiving a great deal of attention for their potential application in flat panel display and illumination [1]. Although an internal quantum efficiency of nearly 100% has been achieved [2,3], due to the mismatch of the refractive index of air, glass substrate, and organic layer, a lot of the generated light is lost through total internal reflection into substrate and indium-tin-oxide (ITO) wave-guiding modes, and to self-absorption. So the external coupling efficiency ($\eta_{\rm ext}$ defined in Eq. (1)) is a critical figure for OLED. The $\eta_{\rm ext}$ is calculated by classical ray optics to be $1/2n^2$, where n is the refractive index of substrate [4]. For glass substrate (n = 1.52), the calculated external coupling efficiency is about 20%, which means 80% of the generated light is wasted. Because of this amazing optical loss in theory, many methods were developed to enhance the efficiency. For example, the surface and edges of glass substrate were roughened to extract the light in the glass substrate, and get a 22% improvement of efficiency [5]. Other methods, such as the spherically shaped patterns [6], the textured meshed surfaces [7], the ordered micro-lens arrays [8,9], the silica micro-spheres [10,11], and the diffusive layer [12-14] were used to reduce the light trapped in the glass substrates. According to the classical ray optics model, the external coupling efficiency can be enhanced by several times by reducing the trapped light. However, contrary to this prediction, the above mentioned methods only achieved an efficiency enhancement of from 22% to 56%.

In fact, the classical ray optics model neglects the interference effect between the reflective electric field and the dipole radiated fields, so the external coupling efficiency is underestimated. In order to analyze the external coupling efficiency accurately, several theoretical models have been developed in previous reports [15–20]. Based on optical interference, a "half-space" dipole model was developed [15], and gave a calculated $\eta_{\rm ext}$ of 26%. In Forrest's report [16], quantum mechanics is used to simulate the behavior of radiating molecules in OLED, and the calculated $\eta_{\rm ext}$ is 56%. In addition, M.-H. Lu developed a combined classical and quantum mechanical microcavity model (CCQMM) [17] and the calculated $\eta_{\rm ext}$ is 23.5%. Recently, the group of Alongkarn Chutinan [18] and Benjamin C. Krummacher [19,20] developed the finite difference time domain method and optical loss mechanisms models to theoretically calculate the $\eta_{\rm ext}$ as about 25%.

The external coupling efficiency ($\eta_{\rm ext}$) cannot be measured directly in experiment. Because of the large absorption coefficients of ITO and organic materials, the light trapped in the ITO/org layer is absorbed before zigzagging to the edges, and can not be collected. Only the light flux of escaped and trapped in the glass substrate can be measured, so the external coupling ratio ($r_{\rm ext}$ defined in Eq. (2)), namely the ratio of the escaped to the sum of the escaped and the trapped emission in the glass substrate, can be more easily obtained in experiment.

In previous reports [15-20], the external coupling efficiency or ratio, was also measured to verify their theoretical results. In M.-H. Lu' work [17], silicon photodiodes on a stage with azimuthally rotation were used to obtain the photon flux of the edge and surface of OLED,

^{*} Corresponding author. E-mail address: zhaoxinwu@mail.xjtu.edu.cn (Z. Wu).

and then obtained $r_{\rm ext}$ of 42% and 32% for Alq₃ based devices with 100 nm and 200 nm ITO thickness respectively [17]; and according to the report of Kim [15], the flux at a given angle was measured by charge coupled device spectrograph, then the total photon flux was obtained by spectral integration, and the $r_{\rm ext}$ is about 52%. More comparisons between the experimental and theoretical results are summarized in Table 1. These different results still did not present us how much generated light can be effectively decoupled from the devices, so further investigations on the external coupling ratio, $r_{\rm ext}$, of OLEDs are required.

In this paper, using the integrating sphere, fiber spectrometer and glass hemisphere, we could directly get the photon flux of the edges and surface of tris-8-hydroxyquinoline aluminum (Alq₃) based OLEDs, then the external coupling ratio, $r_{\rm ext}$ of 56% is obtained. Furthermore, we extended the "half-space" dipole model by taking dipole radiation pattern into account, then calculated the angular distribution pattern of the emission in OLED, and finally obtained the external coupling ratio in theory.

2. Experiment and measurement methods

2.1. The structures of the devices

The OLED structure used in both experiment and modeling is shown in Fig. 1(a). On the glass substrate, the indium-tin-oxide (ITO) layer is used as anode ($n_{\text{ITO}} = 1.9$, thickness = 100 nm, 135 nm, or 170 nm). A copper phthalocyanine (CuPc) thin film with a thickness of 15 nm is used as the hole injection layer, a N,N'-bis (lnaphthyl)-N,N'-diphenyl-1, 1'-biphenyl-4,4'-diamine (NPB) with a thickness of 40 nm is used as a hole transport layer, and a tris-8hydroxyquinoline aluminum (Alq₃, $n_{Alq3} = 1.72$) layer is used as electron transporting and emitting layer; the thickness of Alq₃ is 30 nm, 60 nm, 90 nm, 120 nm, 150 nm, 180 nm for different devices. The 0.8 nm-thick LiF and 80 nm-thick aluminum is the cathode of OLEDs. The glass substrate is $33 \text{ mm} \times 44 \text{ mm}$, $30 \text{ mm} \times 37 \text{ mm}$, $27 \text{ mm} \times 32 \text{ mm}$ or 25 mm × 26 mm, the thickness is 1.2 mm, the four emission areas are all 3 mm×4 mm, and the emission area is at the center of the device. The dimensions of the device are shown in Fig. 1(b). The detailed process of fabrications can be found in our previous publications [21].

2.2. Optical modes and the external coupling efficiency

The optical structure of the device is shown in Fig. 1(c). The emission region is at the interface between the layers of NPB and Alq₃. The emission layer is bounded by the metal cathode and the ITO-glass substrate with an interface with air. Due to the total internal reflection, we can divide the emission light into three modes by their corresponding angular ranges [17].

First, the external modes: when the photons with the internal emission angle θ is in the range: $0 \le \theta \le \theta_1$, $\theta_1 = \sin^{-1}(n_a/n_p)$, the photons will escape from the surface; second, the substrate modes: when the internal emission angle θ is in the range: $\theta_1 < \theta \le \theta_2$, $\theta_2 = \sin^{-1}(n_g/n_p)$, these modes will emerge through the substrate edge after several reflections; lastly, the ITO/organic modes: when the internal emission angle θ is in the range: $\theta_2 < \theta \le \pi/2$, where n_a and n_p are the refractive indices of air and the emitter layer, and n_g is the refractive index of the

glass substrate. And then the external coupling efficiency can be defined by the following equations respectively:

$$\eta_{\rm ext} = {\rm external modes}$$
 (1)
 $/({\rm external modes} + {\rm substrate \ modes} + {\rm ITO/organic \ modes})$

In fact, the absorption coefficient of ITO is on the order of 5000 cm $^{-1}$ [22], so the ITO/organic modes can not be detected from the edges. A part of the substrate modes are absorbed by the OLED when zigzagging to the substrate edges, so the measured value of these modes is underestimated and should be corrected to get the real value. Then the $\eta_{\rm ext}$ can not be measured directly, and only the external coupling ratio $(r_{\rm ext})$ can be obtained as the following equations:

$$r_{\rm ext} = {\rm external modes}/({\rm external modes} + {\rm correctional \ substrate \ modes})$$
 (2)

2.3. Measurement method

In the previous reports [15-17], silicon photodiode (or silicon photodiode arrays) and charge coupled device spectrograph are the most widely used detectors for the electroluminescence (EL) measurements of OLEDs. This can only detect the discrete emission intensity at a given angle, and the discrete values were added to get the total photon flux. It could not directly obtain the flux, and is easy to induce measurement errors. In our research, the photon flux of devices was measured by an integrating sphere (SLM-12,Sphere Optics LLC) combined with a fiber spectrometer (USB 2000+, Ocean Optics Inc.), shown in Fig. 1(d). The diameter of the integrating sphere is 250 cm, which is much greater than the size of the emitting area, and the dimension is suitable for decreasing the instrumental error. And a glass hemisphere is also used in our measurement, which can extract almost all of the substrate modes into external coupling modes. Similar measurement method is also used in other works [23-26]. The fiber spectrometer features high sensitivity, stable quantum efficiency over a certain wavelength range, and near-linear response with the incident light power. And the integrating sphere can collect all of the light emitted from the OLED.

In order to measure the external modes, substrate modes, the "Absorber 1" and "Absorber 2" were used, which is shown in Fig. 1(a). First, the prepared OLED with the edges of the substrate was covered by "Absorber 2," and it was lighted under a given voltage and current, then the measured flux F_1 is external modes; second, with the emitting areas covered by "glass hemisphere," and the then we got the total optical output flux F_{TOT} ; third, the edges of the substrate were covered by "Absorber 2," and the emitting area was still covered by "glass hemisphere," then the measured flux F_1 is the sum of the external modes F_{surf} and the extracted substrate modes F_{edge} ; fourth, with the emitting areas covered by "glass hemisphere" and "Absorber 1," the flux, F_2 , is the sum of unextracted substrate modes, F_{edge} , and ITO/organic modes $F_{\text{TTO/org}}$; lastly, the "Absorber 1," "Absorber 2" and "hemisphere prism" were all covered on all edges and surface of the substrate, and then, the flux F_3 of ITO/organic modes ($F_{\text{TTO/org}}$) could be obtained.

Table 1Summary of the measured and calculated external coupling ratio and conditions in the literature.

Group (or authors)	Measured $r_{\rm ext}$	Calculated $r_{\rm ext}$	Calculated $\eta_{\rm ext}$	Condition
Forrest et al. [16]	62%	61%	56%	ITO (160 nm)/CuPc/α-NPD/Alq ₃ (60 nm)/MgAg
J. Kim et al. [15]	52%	54%	26%	ITO/HTL/small molecule emitting layer/MgAg
M. Lu et al. [17]	42%	38%	23.5%	ITO (100 nm)/PVK/Alq ₃ (60 nm)/MgAg
Noda et al. [18]		40%	25%	ITO (150 nm)/PVK (40 nm)/Alq (60 nm)/Al
Nowy et al. [19]		38%	23%	ITO (50 nm)/Alq (160 nm)/Ca (15 nm)/Al

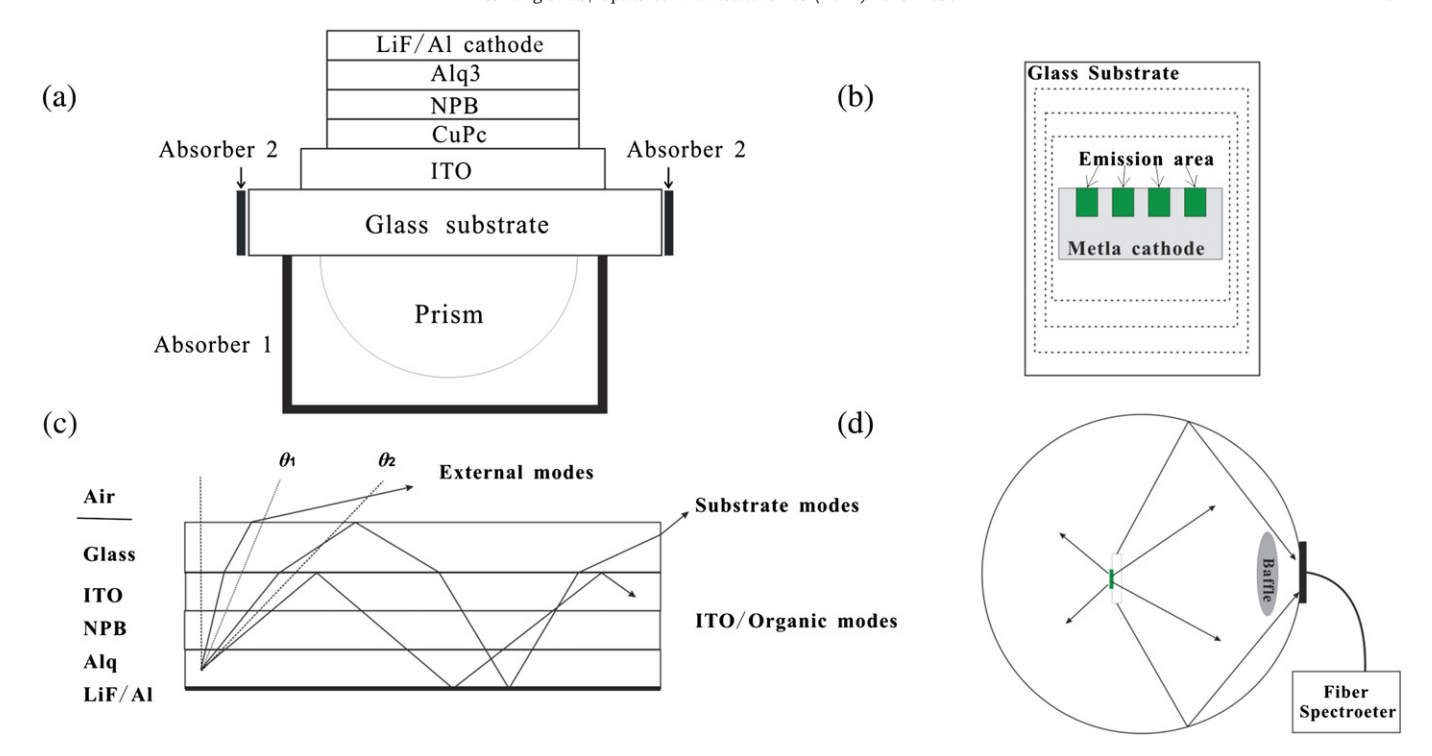


Fig. 1. (a) Schematic diagram of OLEDs and the absorbers; (b) the dimensions profile of the device, the dashed lines are the profiles of other three substrate; (c) schematic diagram showing photons emitted into various modes; (d) schematic diagram of the integrating sphere and fiber spectrometer measurement system.

An index-matching fluid is applied between the hemisphere and the OLEDs, with the same refractive index as the glass substrate, to ensure proper optical contact. In the five steps, the OLED was lightened under the same current density ($r_{\rm ext}$ does not change with current density), and the measurement is rapidly accomplished, so the attenuation of devices is negligible.

The absorption coefficient of ITO and organic material is the order of magnitude of $5000~\rm cm^{-1}$ [22], so the light of the ITO/organic modes can almost not escape the layers before dissipation, and $F_3 = 0$. The absorption of the glass substrate at the wavelength of about 520 nm is very low, and the light is severally reflected at the metal cathode surface when zigzagging to the substrate edges; the metal cathode absorbs a part of energy (Fig. 2). So the real value of the unextracted substrate modes (F_2) can be obtained by retrieving the absorption of metal cathode and glass, and the total flux of the external modes and substrate modes is ($F_1 + F_2$). And then, the external coupling ratio ($r_{\rm ext}$) is calculated by Eq. (3), and it is shown in Fig. 4.

$$r_{\text{ext}} = F_1 / \left(F_1' + F_2'\right)$$
 Glass substrate

Fig. 2. The profile of the devices and the thickness of the glass substrate is 1.2 mm; the black broad-brush represents the metal cathode, and the green broad-brush represents the emission areas. The zigzag line represents the light reflecting on the aluminum cathode.

Metal cathode

Emission area

After the first measurement, we change the glass substrate size as $30 \text{ mm} \times 37 \text{ mm}$, $27 \text{ mm} \times 32 \text{ mm}$, and $25 \text{ mm} \times 26 \text{ mm}$ (in Fig. 1(b)), the emission areas not changing, and remeasure the devices. The results do not alter, so the substrate size does not affect the value of T_{ext} .

3. Results and discussion

3.1. Experimental data

The fluxes of the total emitted light, the external modes, substrate modes, and ITO/organic modes are obtained by the measurement. The external coupling ratio ($r_{\rm ext}$) is calculated by Eq. (2), and it is shown in Fig. 3. The $r_{\rm ext}$ is from 20% to 56%, which varies with the thickness of Alq₃, and there is about 5% measurement error. After the first measurement, we change the glass substrate size as 30 mm×37 mm,

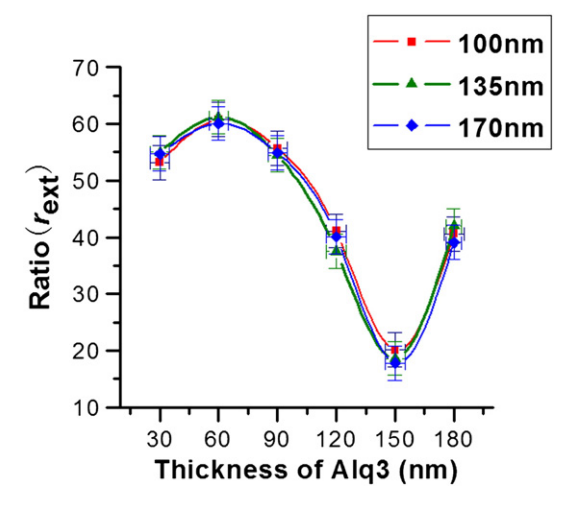


Fig. 3. The measured external coupling ratios of different ${\rm Alq_3}$ and ITO thickness. There is about 5% measurement error.

 $27 \text{ mm} \times 32 \text{ mm}$, and $25 \text{ mm} \times 26 \text{ mm}$ (in Fig. 1(b)), the emission areas not changing, and remeasure the devices. The results do not alter, so the substrate size does not affect the value of r_{ext} .

In addition, from the experiment data, when the thickness of ITO is 100 nm, 135 nm, and 170 nm, the $r_{\rm ext}$ almost does not alter. This phenomenon is consistent with Kim's results [27]. Generally, the number of the optical waveguide modes can be simply calculated by Eq. (4) [28].

$$M = \frac{4d}{\lambda} \sqrt{n_1^2 - n_2^2} \tag{4}$$

Here, d is the thickness of ITO/organic layer, n_1 and n_2 are the refractive indices of ITO/organic layer and glass substrate respectively, and λ is the wavelength of light emitted by Alq₃. From this equation, the ITO/organic layer can only support the zero-order or zero-order and first-order wave-guiding modes for ITO of 100 nm, 135 nm, and 170 nm. Then, only the emitted light at certain angle can couple to zero-order or first-order wave-guiding modes, and the other parts of the light are still in this layer, but can not form wave-guiding modes, and will be dissipated ultimately. So, for the different thickness of ITO, the flux of light emitted to the ITO/organic modes does not alter, and then the intensity of the ITO/organic mode and the external coupling ratio do not alter.

3.2. Extended "half-space" dipole model by taking dipole radiation pattern into account

From the experimental data, our maximal $r_{\rm ext}$ is about 56%, which is a little higher than previous calculations. According to the previous work [15], for the "half-space" dipole model, the light emitted by dipoles is considered as to be isotropic. In fact, the emission of a dipole is not isotropic, its spatial radiation intensity varies with the emission angle [29]. In order to accurately investigate the $r_{\rm ext}$, we extended the "half-space" dipole model by taking dipole radiation pattern into account. In our model, the emission of organic layer is considered as oscillating dipoles emission in front of a mirror [30]. This emission layer is the Alq₃ layer for our devices. These dipoles are embedded inside the emitter half space at a distance z from the mirror (Al cathode-reflector in Fig. 1(a)). The other half space is occupied by the Al cathode. The emission of a dipole is anisotropic, so these dipoles should be divided into three freedoms for calculation, as shown in Fig. 4. This model is also able to represent the interference

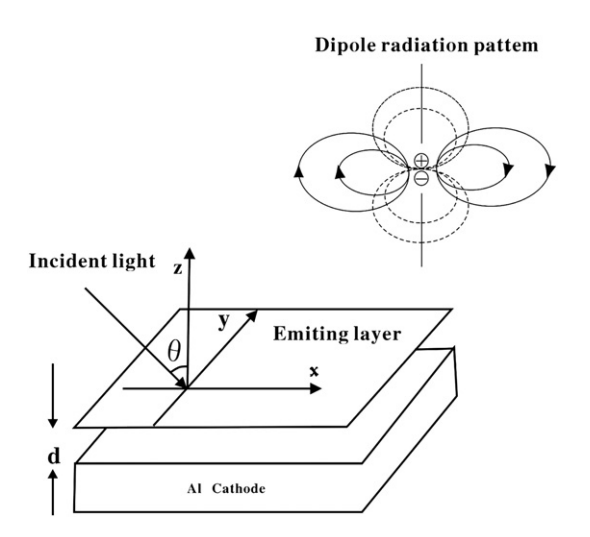


Fig. 4. The schematic diagram of the extended half-space dipole model and the radiation pattern of dipole are on the top right corner.

between the directly emitted light and the light reflected by the metal cathode. And then, it will calculate the angular distribution of the radiation intensity, and then extract the external coupling ratio. In OLEDs, the energy coupled to surface plasmon modes is by the near field effect of dipoles [31,32], so it is nonradioactive losses, and it does not alter the emission patterns of OLEDs. So in our model, we did not take the surface plasmon losses into account.

As shown in Fig. 4., for the emitting dipoles at distance d from the interface of metal cathode and organic layers, the angular distribution for emission intensity (l) of dipoles can be written as the following [30]:

$$I(\theta) = E_1^2 \left| 1 + r_{\rm p} \exp(2i\delta \cos\theta) \right|^2 + E_2^2 \left| 1 - r_{\rm p} \exp(2i\delta \cos\theta) \right|^2$$

$$+ E_3^2 \left| 1 + r_{\rm s} \exp(2i\delta \cos\theta) \right|^2$$
(5)

Here, $r_{\rm s}$, and $r_{\rm p}$ is the Fresnel reflection coefficient for the s- and p-polarization, θ is the internal emission angle and also the direction of the Poynting vector. δ is the phase change incurred in the round trip from the emitter to the organic/cathode interface and back, and $\delta = 2\pi n d/\lambda_0$, where λ_0 is the emission center wavelength in vacuum and n is the refractive index of organic layer. At the x-o-y plane, the angular distribution for emission intensity of x, y, and z dipoles is calculated by $E_1 = P_{\rm e} \sin\theta/4\pi\epsilon r^3$, $E_2 = P_{\rm e} \cos\theta/4\pi\epsilon r^3$, and $E_3 = P_{\rm e}/4\pi\epsilon r^3$ respectively [29], where E is the angular distribution of oscillating dipole emitting, and $P_{\rm e}$ is the electric dipole moment, which is constant for fixed dipole, ε is the dielectric constant of the organic layer, and r is the distance from dipole to a certain point. The curves in Fig. 5 describe the calculated angular emission distribution patterns of the three kinds of dipole freedoms, which change with different Alq $_3$ thickness rapidly.

The calculated dipoles angular emission distributions patterns for small molecule based devices with various thicknesses of Alq_3 are shown in Fig. 5(d). Due to the interference between the directly emitted light and the light reflected by the Al cathode, these patterns obviously alter with the distance from dipoles to the metal cathode.

In order to exactly calculate the photon flux of various modes, the light intensity $(I(\theta))$ is integrated at each angle ranges of the three modes (i.e., $\int_{\text{angle range}} 2\pi \sin\theta \ I(\theta) \ d\theta$), and the photon flux of the various modes is obtained. Fig. 6(a) describes the calculated percentage of the three kinds of modes, and the external coupling efficiency η_{ext} under the different thickness of Alq₃. When the thickness of Alq₃ is 60 nm, the maximal η_{ext} is 43%, and the Alq₃ is 150 nm; only 13% of the light escapes the device, and most of the light is trapped in the device. In addition, the external coupling ratio, r_{ext} , can also be calculated by Fig. 6(a), which was shown in Fig. 6(b), and presented the range of r_{ext} from 20% to 56% under the different thickness of Alq₃. And the calculated results agreed well with our experiments. Our study will benefit the optimization of device structures for the higher out-coupling efficiency.

The external quantum efficiency (η) defined as the number of photons emitted into the viewing direction per injected carrier [33], is expressed in the following equation:

$$\eta = \eta_{\rm int} \eta_{\rm ext} \tag{6}$$

The internal quantum efficiency $(\eta_{\rm int})$ defined as the ratio of the total number of photons generated within the structure to the number of electrons injected. In the small molecule based OLEDs, the maximal $\eta_{\rm int}$ is 25%, and the maximal external quantum efficiency is about

We obtained $\eta_{\rm ext}$ and $r_{\rm ext}$ that are higher than some previous calculations. Fig. 7 shows the comparison of dipoles angular emission distribution patterns, which are calculated by the extended half-space dipole model and the former half-space model respectively, where the thickness of Alq₃ layer is 60 nm. From the comparison, we can

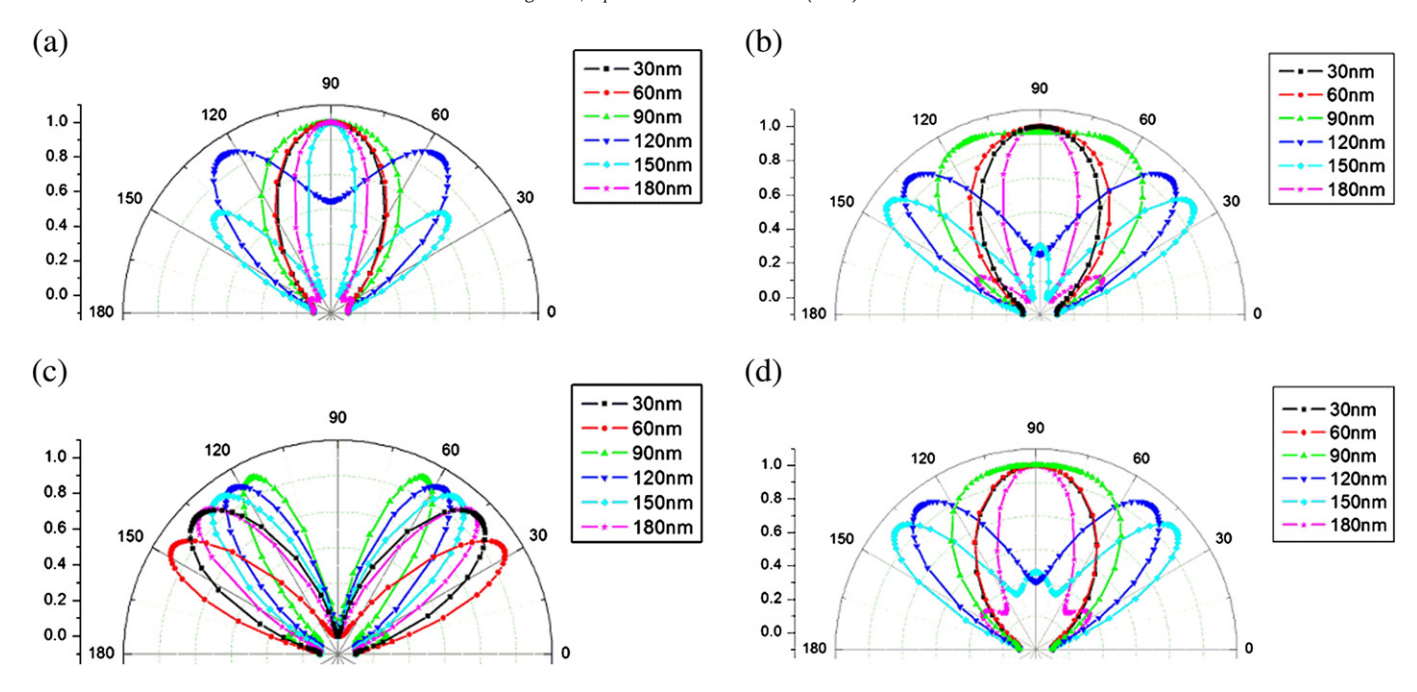
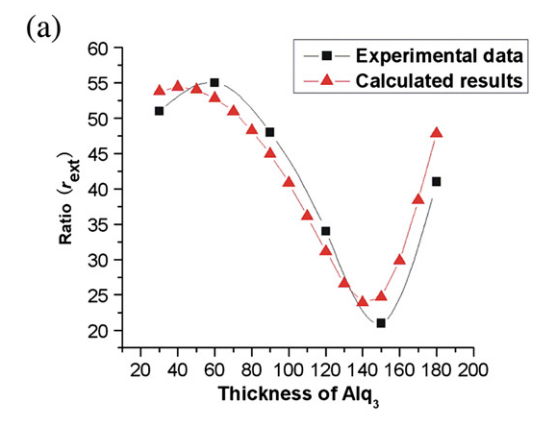


Fig. 5. (a), (b), and (c) are the calculated and normalized angular distributions of emission intensity from dipoles in the *x*, *y*, and *z* directions with different Alq₃ thickness. (d) The calculated and normalized dipoles angular emission distributions patterns for small molecule devices with various thickness of Alq₃ layer.

get that the dipoles radioactive emission at the angle range: $\theta_1 < \theta \le \theta_2$, $\theta_2 < \theta \le \pi/2$ is not as much as the calculation of the former half-space modeling. So the photon flux of the substrate modes and ITO/organic

modes is also not high, and then external coupling ratio or external coupling efficiency obtained by our model is higher than some previous anticipation.



(b) **External modes** Substrate modes ITO/Org modes 55 50 45 Percentage (%) 40 35 30 25 20 15 10 100 Thickness of Alq₃

Fig. 6. (a) The calculated percentage of the three kinds of modes, namely substrate modes, external modes, ITO/organic modes of different Alq₃ thickness. (b) Comparison of the calculated external coupling ratio with experiments.

4. Conclusion

In conclusion, an integrating sphere associating with a fiber spectrometer measurement and an extended "half-space" dipole model by taking dipole radiation pattern into account are developed to describe the external coupling ratio of OLED. We found the maximum external coupling ratio ($r_{\rm ext}$) is about from 20% to 56%, which depends on the thickness of the Alq $_{\rm 3}$ layer. The numerical results are in good agreement with our experiments. These results will benefit researchers to improve the light coupling efficiency and optimize the structure of the small molecule based bottom emitting devices.

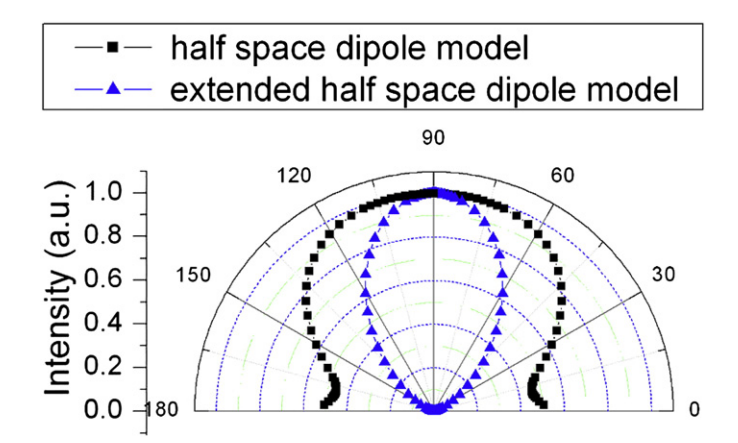


Fig. 7. The dipoles angular emission patterns, which are calculated by the extended "half-space" dipole model and the former "half-space" model respectively.

Acknowledgements

This work was supported by the National Natural Science Young Foundation of China under grant no. 10904122 and by the National Natural Science Key Foundation of China under grant no. 10934001.

References

- [1] S.R. Forrest, Organic Electronics 4 (2003) 45.
- [2] C. Adachi, M.A. Baldo, M.E. Thompson, S.R. Forrest, Journal of Applied Physics 90 (2001) 5048
- [3] B.H. Tong, Q.B. Mei, S.J. Wang, Y. Fang, Y.Z. Meng, B. Wang, Journal of Materials Chemistry 18 (2008) 1636.
- N.C. Greenham, R.H. Friend, D.D.C. Bradley, Advanced Materials 6 (1994) 491.
- [5] S.M. Chen, H.S. Kwok, Optics Express 18 (2010) 37.
- C.F. Madigan, M.H. Lu, J.C. Sturm, Applied Physics Letters 76 (2000) 1650.
- [7] Y.H. Cheng, J.L. Wu, C.H. Cheng, K.C. Syao, M.C.M. Lee, Applied Physics Letters 90 (2007) 3.
- S. Moller, S.R. Forrest, Journal of Applied Physics 91 (2002) 3324.
- [9] M.K. Wei, I.L. Su, Optics Express 12 (2004) 5777.
- [10] T. Yamasaki, K. Sumioka, T. Tsutsui, Applied Physics Letters 76 (2000) 1243.
- [11] F. Li, X. Li, J. Zhang, B. Yang, Organic Electronics 8 (2007) 635.
- [12] T. Nakamura, N. Tsutsumi, N. Juni, H. Fujii, Journal of Applied Physics 96 (2004) 6016.
- [13] J.J. Shiang, A.R. Duggal, Journal of Applied Physics 95 (2004) 2880.
- [14] R. Bathelt, D. Buchhauser, C. Garditz, R. Paetzold, P. Wellmann, Organic Electronics 8 (2007) 293.

- [15] J.S. Kim, P.K.H. Ho, N.C. Greenham, R.H. Friend, Journal of Applied Physics 88 (2000) 1073.
- [16] V. Bulovic, V.B. Khalfin, G. Gu, P.E. Burrows, D.Z. Garbuzov, S.R. Forrest, Physical Review B 58 (1998) 3730.
- [17] M.H. Lu, J.C. Sturm, Journal of Applied Physics 91 (2002) 595.
- [18] A. Chutinan, K. Ishihara, T. Asano, M. Fujita, S. Noda, Organic Electronics 6 (2005)
- [19] S. Nowy, B.C. Krummacher, J. Frischeisen, N.A. Reinke, W. Brutting, Journal of Applied Physics 104 (2008)
- [20] B.C. Krummacher, S. Nowy, J. Frischeisen, M. Klein, W. Brutting, Organic Electronics 10 (2009) 478
- [21] Z.X. Wu, L.D. Wang, Y. Qiu, Chinese Physics Letters 21 (2004) 1370.
- [22] J.S. Kim, P.K.H. Ho, D.S. Thomas, R.H. Friend, F. Cacialli, G.W. Bao, S.F.Y. Li, Chemical Physics Letters 315 (1999) 307.
- J.C. deMello, H.F. Wittmann, R.H. Friend, Advanced Materials 9 (1997) 230.
- Y. He, R. Hattori, J. Kanicki, The Review of Scientific Instruments 71 (2000) 2104.
- [25] Y.T. Hong, J. Kanicki, The Review of Scientific Instruments 74 (2003) 3572.
- [26] S.L.M. van Mensfoort, M. Carvelli, M. Megens, D. Wehenkel, M. Bartyzel, H. Greiner, R.A.J. Janssen, R. Coehoorn, Measuring the light emission profile in organic light-emitting diodes with nanometre spatial resolution, Nature Photonics 4 (2010) 329-335
- [27] S.Y. Kim, J.J. Kim, Organic Electronics 11 (2010) 1010.
- [28] A.W.S., Optical Waveguide Theory, Springer, 1983.
- [29] J.A. Stratton, Electromagnetic Theory, McGraw-Hill, 1941.
- [30] G. Bjork, IEEE Journal of Quantum Electronics 30 (1994) 2314.
- [31] P.A. Hobson, J.A.E. Wasey, I. Sage, W.L. Barnes, IEEE Journal of Selected Topics in Quantum Electronics 8 (2002) 378.
- G. Winter, W.L. Barnes, Applied Physics Letters 88 (2006).
- [33] S.R. Forrest, D.D.C. Bradley, M.E. Thompson, Advanced Materials 15 (2003) 1043.